Experimental Validation of a Mathematical Model for Fixed-Bed Desulfurization

Evangelos A. Efthimiadis and Stratis V. Sotirchos
Dept. of Chemical Engineering, University of Rochester, Rochester, NY 14627

Porous particles of two commercially available ZnO sorbents differing in porosity, surface area, and pore-size distribution were reacted with H_2S at 500 and 600°C in a fixed-bed reactor. Concentration breakthrough curves were determined by analyzing the effluent of the reactor using a gas chromotograph equipped with thermal conductivity and flame photometric detectors. The pore structure of samples collected from different positions in the reactor was analyzed by mercury porosimetry and gas adsorption to determine the variation of the average structural properties of the sorbent with the length of the reactor. The obtained experimental data were used to validate a fixed-bed desulfurization model, which employs detailed submodels for diffusion, reaction, and structure evolution in the porous sorbent particles. With the various parameters appearing in the submodels determined from independent thermogravimetric reactivity evolution experiments, the fixed-bed desulfurization model was found to be capable of providing an excellent description of the behavior of the desulfurization sorbents in a fixed-bed reactor.

Introduction

The tendency of various metal oxides to react with sulfur-containing compounds is used to remove such species (primarily H_2S) from coal-derived gas at high temperatures. Several supported or unsupported oxides, in single or mixed form, have been studied experimentally in the literature as candidate sorbents for hot coal gas desulfurization (for example, see studies by Caillet and Harrison, 1982; Yumura and Furimsky, 1985; Tamhankar et al., 1986; Gangwal et al., 1989; and Efthimiadis and Sotirchos, 1992). In most cases ZnO has been used as one of the active components of the sorbent, since many studies have shown that its use leads to very low equilibrium H_2S concentrations in the exit stream of the desulfurization reactor. Coal gas desulfurization is carried out in fixed-bed reactors, but other reactor configurations, such as moving and fluidized-bed reactors, are currently under study and development (Jain et al., 1990; and Lee et al., 1990). Fixed-bed reactors are also used almost exclusively in experimental studies of the performance of coal gas desulfurization sorbents.

Mathematical models for fixed-bed reactors are very useful in design and scale-up studies, especially if they are capable of predicting the behavior of these units for different conditions from those at which they were tested and validated. They are also indispensable for the analysis of experimental data from lab-scale fixed-bed reactors employed in laboratory studies since, because of the very high rate of reaction of metal oxides with H_2S, it is practically impossible to achieve differential operation of such reactors. Desulfurization in fixed beds is a complex process requiring consideration of a large number of subprocesses for its description. One has to consider mass transport in the particles, mass transport through the product layer formed in the interior of the particles, reaction at the unreacted-reacted solid interface, and evolution of the physical microstructure of the reacting particles. Since the concentrations of sulfur-containing pollutants in coal gas streams are typically low, small amounts of heat are released during the reaction, and consequently, consideration of heat transport is not necessary for the description of the process. A mathematical model for a fixed-bed desulfurization reactor, therefore, consists of three submodels, one for describing mass transport and reaction in the bed, another for mass transport and reaction in the particles, and a third for local reaction and structure evolution within the particle or pellet.

The equations for mass transport and reaction in the fixed bed are relatively well-defined. Thus, what really differentiates

Correspondence concerning this article should be addressed to S. V. Sotirchos.

one fixed-bed model from another is the submodel used to describe the behavior of the individual sorbent pellets or particles in the bed. If one wants to avoid the complication of developing a theoretical single pellet model and testing it, the only available alternative is to use experimental data for single pellets or differential reactors to develop an experimental single pellet model, that is, a correlation for the dependence of the average reaction rate of the pellets (or particles) on solid conversion, temperature, and reactant concentration. Of course, such a model will be useful only if the conditions used in the operations of the fixed bed are within the range used to develop the experimental model. Such an approach was taken, among others, by Park et al. (1984) in their study of the oxidation of reduced iron oxide with water vapor, a problem fundamentally similar to that of metal oxide sulfidation.

The performance of a mathematical model for coal gas desulfurization in fixed beds is examined in this study. The mathematical model is developed along the lines of the fixed-bed desulfurization model by Sotirchos and Zarkanitis (1989). The random pore and grain models of Sotirchos and Yu (1985, 1988) for gas-solid reactions with solid product were used by Sotirchos and Zarkanitis to describe the behavior of individual pellets, but in our model we will make use of the generalized random pore model of Yu and Sotirchos (1987). This is a model for reaction and structure evolution in porous media of pore-network structure undergoing a gas-solid reaction with solid product. Past studies on the sulfidation of two zinc oxide sorbents in a thermogravimetric analysis system (Efthimiadis and Sotirchos, 1992) showed that this structural model can successfully describe the behavior of single particles over a broad range of operating conditions. The fixed-bed desulfurization model is evaluated using experimental data for sulfidation of ZnO sorbents in a fixed-bed reactor, obtained in our laboratory at various combinations of operating conditions using the same two sorbents used in our past studies. No adjustable parameters are used in the comparison of model predictions and experimental data since all parameters needed for the description of individual particles using the generalized random pore model have been determined independently from thermogravimetric analysis data.

Materials

The sorbents used in this study were mixtures of metal oxides with ZnO being the main constituent and other compounds (Al_2O_3, SiO_2, CaO, and MgO) being present in smaller amounts. The fresh materials were obtained from United Catalysts in the form of 3/16 in. extrusions with the commercial names: catalysts G-72D and C7-2. The unreacted materials showed some weight loss during heat treatment under nitrogen flow, most probably caused by removal of volatile compounds (binder solid and humidity). For this reason, the unreacted solids were heat treated for 30 min at 600°C before each sulfidation experiment. The compositional analysis of the two sorbents showed that 89% of sample G-72D and 78% of sample C7-2 on a weight basis (after heat treatment) was zinc oxide. The rest was mainly alumina and silica in sample C7-2 and alumina in sample G-72D. The extrusions were crushed and divided into particle-size ranges using mechanical sieving.

Particles of 297–350 μm were used in the characterization of the pore structure of the solids. In Table 1 we summarize the physical properties of the unreacted heat-treated materials. Pores in the range of 10,000–20 Å were accounted for in the estimation of the pore volumes of Table 1 that were obtained from the mercury porosimetry data. The physical properties of the micropores (pores of radius less than 20 Å) were computed using the t-method (De Boer et al., 1965). The small micropore volume and surface area of both materials and the pore-size distributions of the solids (to be presented later in Figures 13 and 14) showed that the pore space of both samples consists primarily of mesopores (pores with radius in the range 20–500 Å) and macropores (pores with radius larger than 500 Å). The BET surface area of the two sorbents is almost the same, but there is a significant difference in their pore volumes and most probable pore radii. (The most probable radius is the value where the slope of the cumulative pore volumes vs. pore radius curve has its maximum value.) Sample C7-2* corresponds to a different batch of catalyst C7-2. It can be seen from the Table 1 that there are negligible differences between the physical properties of the two batches of sample C7-2. Moreover, when samples of the two batches were sulfided under identical reaction conditions, the conversion vs. time curves were within experimental error identical. A detailed investigation of the pore structure of unreacted sorbents G-72D and C7-2 and their sulfides was carried out in another study by Efthimiadis and Sotirchos (1992b).

Apparatus and Procedure

Sulfidation experiments were carried out isothermally in a fixed-bed reactor system, which is shown in Figure 1. The reactor was a quartz tube of 1.5 or 0.75 cm I.D. mounted vertically in a 3-zone furnace, which maintained a uniform temperature profile in the reactor. The sorbent was placed in the quartz tube between two zones of spherical quartz beads (1 mm in diameter) of about 2 cm in height each. The sorbent bed was supported by quartz wool placed at the bottom of the lower zone of quartz beads and at the top of the upper zone. The configuration of the reactor allowed the measurement of the reactor temperature using two thermocouples, one introduced through the upper fitting of the tube, as shown in Figure 1, and the other through the fitting at its bottom. In a typical

Table 1. Physical Properties of Unreacted Heat-Treated Sorbents

Zinc Oxide Sample	G-72D	C7-2	C7-2*
Total Pore Volume (Hg porosimetry), cm^3/g	0.178	0.289	0.275
BET Surface Area, m^2/g	26.57	27.72	25.52
Most Probable Radius (Hg Porosimetry), Å	115	200	200
Most Probable Radius (N_2 Adsorption), Å	125	180	200

*Second batch of sorbent C7-2.

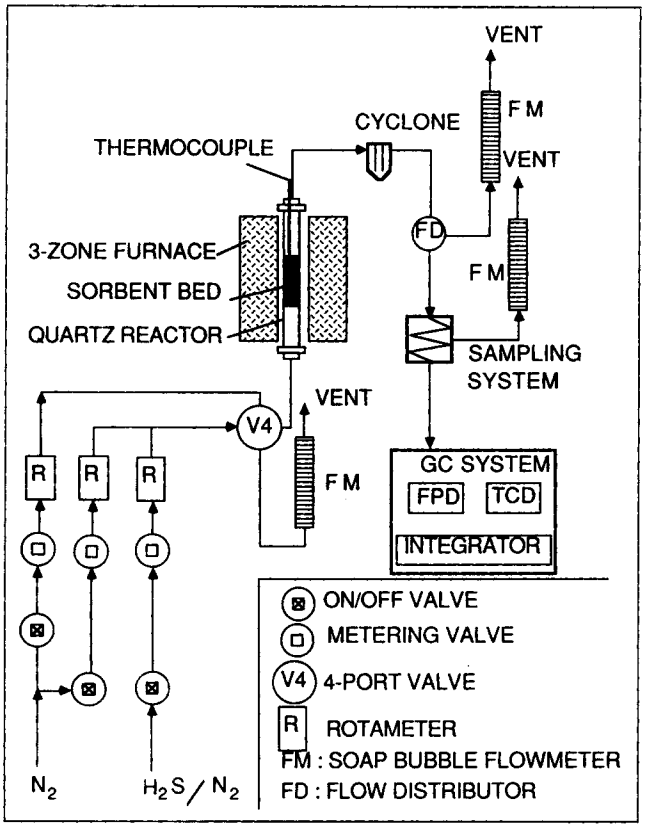

Figure 1. Schematic of the fixed-bed reactor and the gas analysis system.

experiment, the thermocouple tips were placed outside the bed at a distance of a few mm from the quartz wool. However, in two runs the upper thermocouple was placed in the middle of the sorbent bed in order to measure the variation of the temperature in the sorbent bed during the reaction. The temperature difference between the indication of this thermocouple and that at the entrance of the reactor was less than 3°C at all times, implying that small amounts of energy were released by the exothermic reaction at the reaction conditions of our study.

The fixed-bed reactor of Figure 1 was loaded with particles of 210-250, 297-350 and 710-850 μm. The bed voidage was computed from the dimensions of the sorbent bed, the weight of the solid, and the bulk density of each sorbent (2.7 g/cm^3 for sample G-72D and 2.0 g/cm^3 for sample C7-2), the latter determined from the skeletal density and porosity of the unreacted materials. It was found that the bed voidage was approximately 40% for the two reactor tubes and for all particles sizes used in this study. This value agrees with the experimental data of Dixon (1988) on the dependence of the void fraction in fixed beds on the particle to tube diameter ratio.

The gas distribution system involved a system of on/off and metering valves, arranged to control the flow rate and composition of the gas stream entering the reactor. The reactive gas was a mixture of 10,500 ppm H_2S in nitrogen, which could be further diluted with nitrogen, as shown in Figure 1. Standard correlations for flow through particle beds were used to estimate the pressure drop in the bed; it was found to be negligible for all particle sizes and conditions used in our studies. The gas stream leaving the reactor was divided into two streams. The first (about 90-95% of the main stream) was sent to the vent, while the second was used for gas analysis by sending it through the sampling loop of the injection system of a chromatograph. The injection system consisted of a 6-port valve attached to an electric actuator. A programmable integrator (Chromjet of Spectra Physics) was used for automatic injection and analysis of gas samples every 3 min. The same reactor configuration could also be used for fluidized-bed experiments. Much larger flow rates were used to fluidize the particles during such experiments. The cyclone in Figure 1 was used to separate and collect the fines produced by attrition of the sorbent particles during fluidization.

The gas chromatograph was a Varian 3300 equipped with FPD and TCD detectors. The analysis was carried out isothermally at 90°C with helium as the carrier gas. Preliminary experiments showed that there was a linear relation between the square root of the integrated H_2S peak and the concentration of the injected samples when the H_2S content of the stream was lower than 2,000 ppm. Thus, low H_2S concentrations were detected by the FPD, while higher H_2S concentrations were measured by the TCD, which could also detect nitrogen and water vapor. The weight of the sulfided sorbent was measured at the end of the experiment, and its difference from the initial sorbent weight (after the loss of the volatile compounds) was used to estimate the average conversion of the sorbent in the bed. This value was, within 1% error, in agreement with the average conversion determined from the variation of the H_2S concentration of the effluent stream of the reactor with time. Samples of reacted material were collected from different parts of the bed and were analyzed by mercury porosimetry and gas adsorption (N_2 at 77 K). A Micromeritcs Autopore II 9220 mercury porosimeter and a Quantachrome Autosorb 1 volumetric adsorption unit were used for the characterization of the samples.

Single Particle Behavior

Gas-solid reactions of the form *Solid + Gas → Solid + ...*, with ... denoting other gas species participating in the reaction, were modeled by Yu and Sotirchos (1987) in the so-called generalized random pore model. This model accounts for structural changes in the interior of the porous solid, diffusion of the gas species in the pore space and in the product layer, and chemical reaction at the interface between the unreacted and the sulfided solid. The pore space of the solid is assumed to consist of cylindrical pore segments arranged in the form of a three-dimensional lattice. The population of pores is described using the experimentally determined pore-size distribution of the unreacted solid (from mercury intrusion data). The equations describing structural changes in the interior of the solid reactant with the progress of the reaction and variation of the intraparticle diffusion coefficient with the local conversion in the particle can be found in the works of Yu and Sotirchos (1987) and Zarkanitis et al. (1990).

The equations that describe diffusion of a gaseous species in a spherical porous particle and reaction with the solid are written using dimensionless quantities as follows:

$$\frac{\partial(\omega_p \epsilon_p y_p)}{\partial \tau_p} = \frac{1}{\Phi^2}\frac{1}{\rho^2}\frac{\partial}{\partial \rho}\left(\rho^2 \frac{\partial}{\partial \rho}(\delta^e y_p)\right) - \nu_A \kappa_w y_p \qquad (1)$$

$$\frac{\partial \xi}{\partial \tau_p} = \frac{1}{(1-\epsilon_0)} \kappa_v y_p \tag{2}$$

y_p is the concentration of the reactive gas, ρ is the radial distance in the particle, δ^e is the effective diffusivity, κ_v is the volume-based reaction rate constant, ϵ_0 and ϵ_p are the porosities of the unreacted and reacted particle, respectively, ξ is the local conversion of the particle, ν_A is the stoichiometric coefficient of the reactive gas, and τ_p is the time. Equations 1-2 are written for the first-order reaction with respect to the gaseous reactant, since this was found to be the case for the reaction of sorbents G-72D and C7-2 with H_2S in our previous studies (Efthimiadis and Sotirchos, 1991). The boundary and initial conditions for Eqs. 1 and 2 are:

$$\frac{\partial y_p}{\partial \rho} = 0 \Big|_{\rho=0}; \quad \frac{Sh^e}{\delta^e}(1-y_p) = \frac{\partial y_p}{\partial \rho}\Big|_{\rho=1} \tag{3a,b}$$

$$y_p = 0 \text{ and } \xi = 0 \text{ at } \tau_p = 0 \tag{4a,b}$$

The dimensionless quantities shown in Eqs. 1-4 are defined by the equations:

$$\rho = \frac{r}{a}; \quad y_p = \frac{c_p}{c_b}; \quad \delta^e = \frac{D^e}{D_0^e}; \quad \kappa_v = \frac{k_v}{k_{v0}} \quad \omega_p = v_s c_b \tag{5a-e}$$

$$\tau_p = v_s k_s S_0 \int_0^t c_b dt'; \quad \Phi^2 = a^2 \frac{k_s S_0}{D_0^e}; \quad Sh^e = \frac{k_g a}{D_0^e} \tag{6a-c}$$

The symbols used in Eqs. 5 and 6 are explained in the notation section of this article.

Experimental data obtained during the sulfidation of G-72D and C7-2 particles of 53-350 μm were used in previous studies (Efthimiadis and Sotirchos, 1992) to test the applicability of the generalized random pore model to zinc oxide sulfidation. Excellent agreement was found to exist between model predictions and experiment. However, in some of the fixed-bed experiments, the C7-2 particles were larger than those used in our previous sulfidation studies. Therefore, additional sulfidation experiments were performed in the thermogravimetric analysis (TGA) system using particles of 600-710 and 710-850 μm. C7-2 samples of about 3 mg were reacted with 0.5% H_2S diluted in nitrogen at 200 ml/min flow rate (at standard conditions). Details about the TGA reactor are given elsewhere (Efthimiadis and Sotirchos, 1992a). The TGA experimental data were successfully reproduced by the generalized pore model without using any adjustable parameters since the two parameters needed for the application of the mathematical model (diffusion coefficient in the product layer and coordination number of the pore network (that is, average number of pores per node) had been determined in previous studies (Efthimiadis and Sotirchos, 1992a) by fitting the model predictions to the experimental data for particles in the size range 53-350 μm. Experimental and predicted conversion vs. time curves for sulfidation at 600°C of C7-2 particles in the size range 210-850 μm are shown in Figure 2.

In the sulfidation of ZnO sorbents, as well as in most gas-solid reactions, the time associated with structural changes in the interior of the particles is much larger than the time associated with the establishment of the steady-state profile of

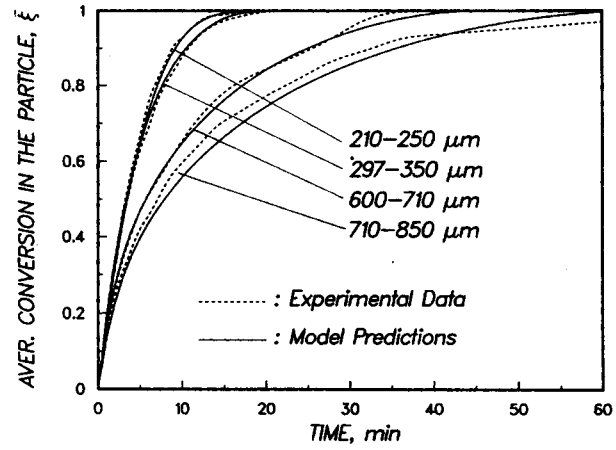

Figure 2. Comparison of thermogravimetric reactivity data at 600°C with the mathematical model predictions.

the reactive gas concentration in the particles (pseudosteady-state approximation). As a result, the transient term in Eq. 1 can be set equal to zero. The average reaction rate per unit of particle volume, $\bar{R}_v$, is then related to the concentration of H_2S in the surrounding gas phase (that is, in the bed) by the equation:

$$\bar{R}_v = \bar{k}_v(\bar{\xi}) c_b \tag{7}$$

The average conversion of a particle ($\bar{\xi}$) and the average volumetric reaction rate constant in a particle ($\bar{k}_v(\bar{\xi})$) can be computed from the local conversion (ξ) and reaction rate constant ($k_v(\xi)$) using the equations:

$$\bar{\xi} = \int_0^1 \xi d\rho^3 \tag{8}$$

$$\bar{k}_v(\bar{\xi}) = \int_0^1 k_v(\xi) y_p d\rho^3 \tag{9}$$

Shown in Figure 3 is the variation of the volumetric reaction rate constants with the conversion at 600°C for various particle sizes of the two sorbents used in our experiments. The evolution of the average volumetric reaction rate with the average conversion in particles sulfided at 500°C was similar to that of Figure 3. The volumetric reaction rate constants in Figure 3 were normalized with respect to the initial volumetric reaction rate constant in the absence of intraparticle diffusional limitations ($k_{v0} = k_s S_0$). Therefore, the initial value of $\bar{k}_v(\bar{\xi})/k_{v0}$ is equal to the initial effectiveness factor, and as a result, in the absence of initial intraparticle diffusional limitations it should be unity. Increasing the particle size intensifies the intraparticle diffusional limitations and leads to lower average reaction rate for the same average conversion in the particle. According to the results of Figure 3, the average reactivity of sorbent G-72D not only is lower than that of sorbent C7-2 (same size particles) but decreases faster with the conversion as well. As the results of Table 1 show, sample G-72D has less pore volume per unit mass and smaller most probable radius than sample C7-2. Moreover, it was found from the analysis of the single

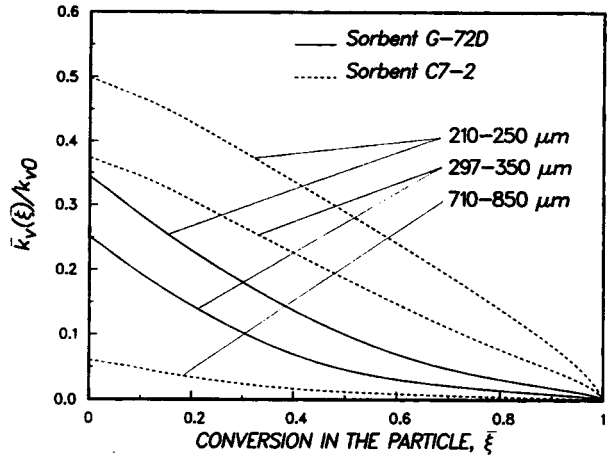

Figure 3. Evolution of the average volumetric reaction rate constant with the average conversion in various particle sizes at 600°C.

particle sulfidation data that the effective diffusivity of H_2S in its pore space is smaller and decreases faster with the conversion than that in sample C7-2 (Efthimiadis and Sotirchos, 1992b).

Mathematical Model for a Fixed-Bed Reactor

The development of a mathematical model for a fixed-bed reactor is facilitated greatly by assuming that the concentration in the bed changes negligibly within a distance equal to the particle or pellet size. The average local reaction rate and conversion at any point in the bed are then equal to the average reaction rate and conversion of a particle, which experiences ambient conditions identical to those at the same point of the bed. The average local reaction rate and conversion in the bed are given by Eqs. 8 and 9, and as a result, it is necessary to solve the structural and particle model equations at every point in the bed in order to determine their values. For a first-order reaction—as it is the case here—it is not necessary to solve these two models simultaneously with the bed equations if the pseudosteady-state approximation is used for diffusion in the product layer and diffusion and reaction in the pore space. The structural model is solved first to create a database for the particle problem, which is then solved to create a database (for the variation of $\bar{k}_v$ with $\bar{\xi}$) for the bed model. This approach was used by Sotirchos and Zarkanitis (1989) in their fixed-bed desulfurization model.

The equations that describe the material balances of the gas and the solid reactant are in dimensionless form:

$$\epsilon_b \frac{\partial y}{\partial \tau} = \frac{\partial^2 y}{\partial x^2} - Pe \frac{\partial y}{\partial x} - \bar{\Phi}^2(\bar{\xi}) y \tag{10}$$

$$\frac{\partial \bar{\xi}}{\partial \tau} = \omega \bar{\Phi}^2(\bar{\xi}) y \tag{11}$$

where

$$y = \frac{c}{c_0}; \quad x = \frac{z}{L}; \quad Pe = \frac{uL}{D_b} \tag{12a,b,c}$$

$$\tau = \frac{tD_b}{L^2}; \quad \bar{\Phi}^2(\bar{\xi}) = \frac{(1-\epsilon_b)L^2 \bar{k}_v(\bar{\xi})}{D_b}; \quad \omega = \frac{v_s c_0}{(1-\epsilon_0)(1-\epsilon_b)} \tag{13a,b,c}$$

y is the concentration of the reactive gas in the bed, x is the axial distance in the bed, ϵ_b is the bed voidage, $\bar{k}_v(\bar{\xi})$ is the volumetric reaction rate, Pe is the Peclet number, and τ the reaction time. The symbols in Eqs. 12 and 13 are given in the notation section of this article. The boundary and initial conditions used for Eqs. 10 and 11 are:

$$-\frac{\partial y}{\partial x} = Pe(1-y) \text{ at } x = 0 \tag{14}$$

$$\frac{\partial y}{\partial x} = 0 \text{ at } x = 1 \tag{15}$$

$$y = 0 \text{ and } \bar{\xi} = 0 \text{ at } \tau = 0 \tag{16a,b}$$

The numerical procedure followed for the solution of the above equations is described in detail by Sotirchos and Zarkanitis (1989).

Before we proceed with the presentation of the model predictions, we will briefly discuss some of the assumptions made in the development of the mathematical model for the bed. No energy balance was included in the bed model since the reactor was assumed to operate isothermally. As mentioned previously, the temperature rise in the bed was too small (less than 3°C) to justify use of a nonisothermal model. It is assumed that the bed voidage (ϵ_b) remains constant during the sulfidation reaction. Even though the solid product occupies more space than the solid reactant, this assumption is not unreasonable because reaction mainly occurs in the interior of the porous particles. The ratio of the internal surface area of the solids to the geometrical external surface area is about 4,000 for particles of 200 μm and larger for the other particle sizes used in this work. The axial dispersion coefficient, D_b, was estimated from the formula $D_b = \epsilon_b \mathfrak{D}/\eta$ for $\eta = 2$. $\mathfrak{D}$ is the binary diffusion coefficient of H_2S in N_2, and η is the tortuosity factor of the bed. We chose to work with this value of axial dispersion coefficients on the basis of the pulse chromatographic studies of Krishnan and Sotirchos (1990) for beds packed with calcium oxide particles of same size as those used in our experiments.

The predictions of the mathematical model were found to be strongly influenced by the type of sorbent, size of sorbent particles, and residence time of reactive mixture in the sorbent bed. Figure 4 presents simulation results for the reaction of 210-250 and 297-350 μm particles of samples G-72D and C7-2 with a mixture of 10,500 ppm H_2S in nitrogen at 600°C. The reaction times were normalized with respect to the minimum time required for complete conversion of the bed (t_0). The space velocity for all the cases of Figure 4 was 20,000 h^{-1} (based on the volume of empty bed at standard conditions), and the reactor diameter and length were 0.75 and 3.40 cm, respectively. For small H_2S concentration in the exit stream, t/t_0 gives a direct measure of sorbent utilization (sorbent used/initial bed load) in the bed. According to the results of Figure 4, the sorbent utilization decreases with increasing particle size for a given breakthrough concentration. Moreover, it takes

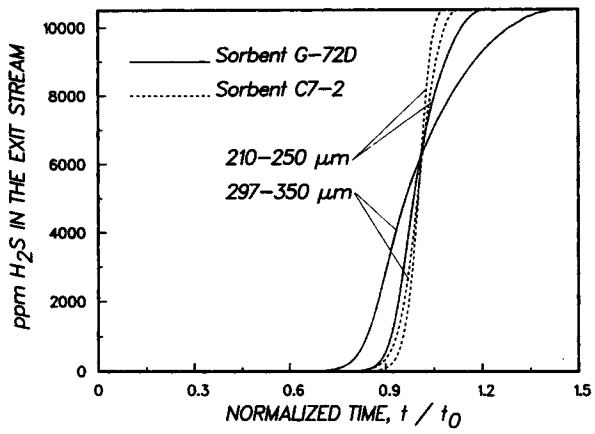

Figure 4. Breakthrough curves predicted by the mathematical model for sulfidation at 600°C of sorbent beds loaded with zinc oxide particles.

less time to get a certain concentration at the exit of the reactor when the reactor is loaded with G-72D particles.

The conversion profiles in the reactor for the four cases of Figure 4 are shown in Figure 5 at reaction times 0.3, 0.6, and 0.9 (t/t_0). Because of the high value of space velocity used to obtain the results of Figure 4, the contribution of the axial dispersion term in the mass balance in the bed is negligibly small. As a result, with the exception of the early stages of the reaction, the concentration profiles in the bed are identical to those of Figure 5. The behavior of the results of Figures 4 and 5 for the breakthrough curves are in agreement with those of Figure 3 for the variation of the volumetric reaction rate constant. (The k_{v0} values for the two sorbents do not differ significantly.) The sorbent utilization for a certain breakthrough concentration varies in the same order as the average reactivity of the particles, and the spread of the conversion profile in the bed increases with decreasing particle reactivity.

The performance of a sorbent bed loaded with 297–350 μm particles at 600°C, under different reactive gas flow rates corresponding to space velocities (S.V.) of 20,000, 10,000, and 2,000 h^{-1} (at standard conditions) is examined in Figure 6. The dimensions of the sorbent bed are the same as those in Figure 4. Large residence times (small reactive gas flow rates) tend to reduce the spread of the conversion profile in the reactor and, hence, increase the utilization of the sorbent at the breakthrough point. Obviously, there is a trade-off between gas throughput in the reactor and sorbent utilization. Therefore, the conditions for optimal operation depend not only on the sorbent but on the economics of the overall process (sulfidation and regeneration) as well.

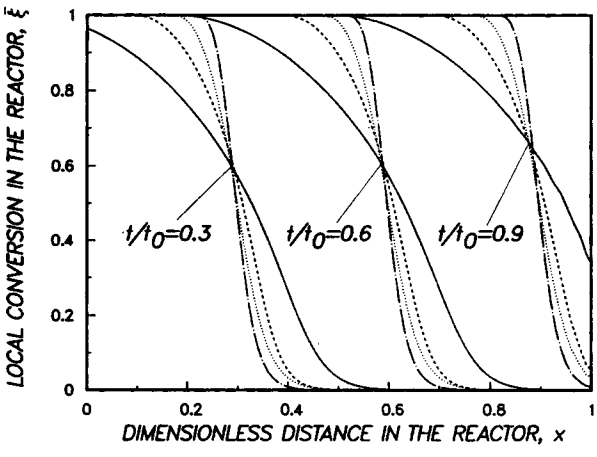

Figure 5. Conversion profiles in the sorbent bed at different reaction times for the cases presented in Figure 4.

——: G-72D, 297–350 μm; — — —: G-72D, 210–250 μm; · · · · ·: C7-2, 297–350 μm; —·—: C7-2, 210–250 μm.

Sulfidation Experiments in a Fixed-Bed Reactor and Model Predictions

In this section, we present and discuss the breakthrough curves that were measured in our experiments and compare them with the predictions of the mathematical model. The application of the model involves no unknown parameters. The parameters of the sorbent bed (particle diameter, weight of the unreacted solid, and bed length and radius) and the operating conditions (temperature and reactive gas flow rate and composition) are directly measured. On the other hand, the parameters for the particle model (diffusion, reaction, and structure evolution equations)—which are needed to determine $\bar{k}_v(\bar{\xi})$ (using Eqs. 8 and 9)—are found from the analysis of the single-particle TGA reactivity data. Table 2 summarizes the reaction conditions for the various fixed-bed experiments discussed in this section. The reactive mixture was 1.05% H_2S in N_2 for all experiments, with the exception of run FB209, where a mixture containing 0.509% H_2S was used.

It should be pointed out that in addition to the particle sizes listed in Table 2, experiments were also carried out with 53–62 and 88–105 μm particles under various reaction conditions. It was observed that particles in these size ranges tended to agglomerate in the fixed-bed reactor, leading to significant pressure drop in the reactor. Problems of this kind were not encountered in beds loaded with particles larger than 200 μm.

No H_2S was detected by the flame photometric detector (FPD) before the breakthrough point in all our experiments, implying that the H_2S concentration in the exit stream of the reactor was below the detection limit of the detector (about 1

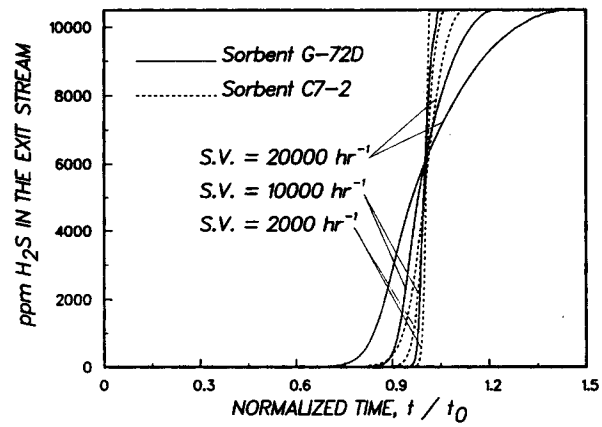

Figure 6. Effect of the space velocity (S.V.) of the reactive gas on the model predictions for sulfidation of 297–350 μm particles at 600°C.

Table 2. Reaction Conditions Used in the Sulfidation Experiments

Run	Sorbent	Particle Size μm	Reactor ID cm	Reactor Length cm	Temp. °C	Space Vel. h^{-1}
FB107	G-72D	297-350	0.75	2.8	500	5,120
FB105	C7-2	297-350	0.75	2.8	500	4,920
FB104	G-72D	297-350	0.75	2.5	600	5,395
FB101	C7-2	297-350	0.75	2.8	600	4,880
FB102	C7-2	210-250	0.75	2.8	600	4,790
FB209	G-72D	210-250	1.5	2.5	600	14,620
FB108	G-72D	297-350	0.75	2.5	600	1,995
FB106	C7-2	297-350	0.75	2.5	600	2,070
FB212	G-72D	297-350	1.5	5.4	600	1,850
FB211	C7-2	297-350	1.5	2.5	600	16,120
FB301	C7-2	710-850	1.5	9.4	600	3,050
FB302	C7-2	710-850	1.5	8.7	600	3,320

ppm). The equilibrium concentration for the reaction of ZnO with 10,500 ppm H_2O in nitrogen at 500 and 600°C was calculated using thermodynamic data from Barin and Knacke (1973). In accordance to our gas analysis measurements, lower H_2S concentrations than our detection limit (for example, 0.4 ppm at 600°C) were estimated from the thermodynamic calculations.

The experimental and theoretical results of Figure 7 give breakthrough curves for samples G-72D and C7-2 at 500 and 600°C. The experimental data (the H_2S concentrations measured by GC analysis) are given by distinct points, while the model predictions are presented as continuous curves. (The results will be presented in the same way in all the other figures we will discuss in this section.) The experiments of Figure 7 were performed using particles of 297-350 μm and space velocities of about 5,000 h^{-1}. Very good agreement, both qualitative and quantitative, appears to exist between model and experiment in Figure 7. This was found to be true for all cases considered in our study, a remarkable result considering that all model parameters were determined from independent experiments. Relatively large deviations between the theoretical and experimental results were observed only for small breakthrough concentrations, that is, in the vicinity of the 'elbow'

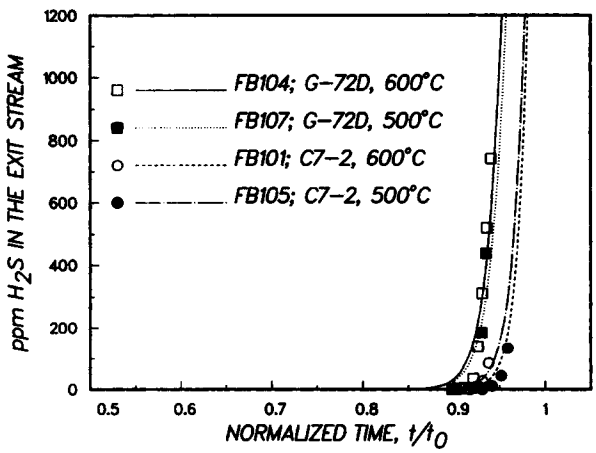

Figure 7. Comparison of the experimental data with the model predictions at different reaction temperatures.

of the breakthrough curve. Even if the data for small concentrations were as reliable as those for large concentrations, this behavior should not surprise us. The sulfidation of zinc oxide is a reversible reaction, and it is thus possible that the actual kinetics for small concentration values is much different from the irreversible, linear kinetics used in the mathematical model.

The results of Figure 7 indicate that the reaction temperature has almost no effect on the experimental and theoretical data. This is in agreement with the weak effect of desulfurization temperature on the behavior of single C7-2 and G-72D particles that we observed in our TGA studies (Efthimiadis and Sotirchos, 1991). Weak influence of desulfurization temperature on the experimental data was also seen in fixed-bed experiments of other desulfurization studies such as the study of Yumura and Furimsky (1985) with zinc oxide sorbents and Gangwal et al. (1989) with zinc ferrite sorbents. We did not cover a larger temperature range in our experiments, because at temperatures higher than 600°C we may have sintering and zinc loss (above 650°C according to Tamhankar et al. (1986) and Gangwal et al. (1989)), whereas at temperatures below 500°C reactivity results may be corrupted by sulfur chemisorption in the sorbents (Efthimiadis and Sotirchos, 1992).

Since the residence time of the reactive mixture in the sorbent bed has strong effects on sorbent utilization (Figure 6), experiments were carried out in the fixed-bed reactor of Figure 1 over a broad range of space velocities (about 2,000-15,000 h^{-1}). The experimental data and the model predictions for a bed loaded with particles of the G-72D sample and sulfided at 600°C are shown in Figure 8. Particles of 210-250 μm size were used in the FB209 run, while in all the other runs the reactor was loaded with 297-350 μm particles. The dependence of the breakthrough response of the fixed-bed desulfurization reactor on particle size and space velocity may also be seen in Figure 9 for beds loaded with sample C7-2 but for a much broader range of particle size than for sample G-72D (Figure 8). In agreement with the theoretical predictions of Figures 4 and 6, the results of Figures 8 and 9 show that an increase in the particle size or in space velocity increases the spread of the breakthrough curve and leads to lower sorbent utilization. It is interesting to note that a combination of smaller particle size and higher space velocity in run FB209 relative to the values used in run FB104 produces a breakthrough curve similar to that obtained in the latter case. The H_2S concentration used in run FB209 is half the value used in all other experiments

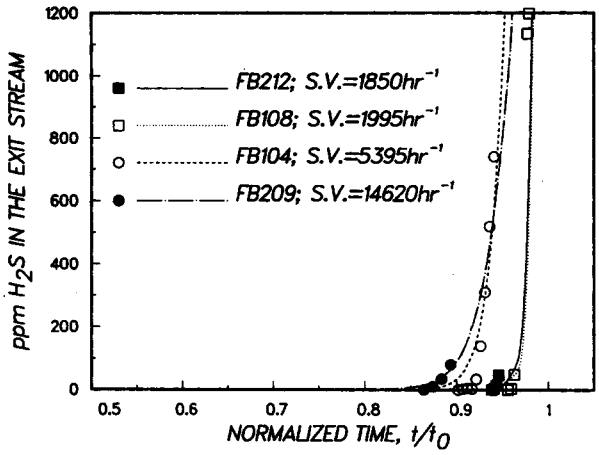

Figure 8. Experimental data and model predictions for sulfidation of the G-72D sample at 600°C.

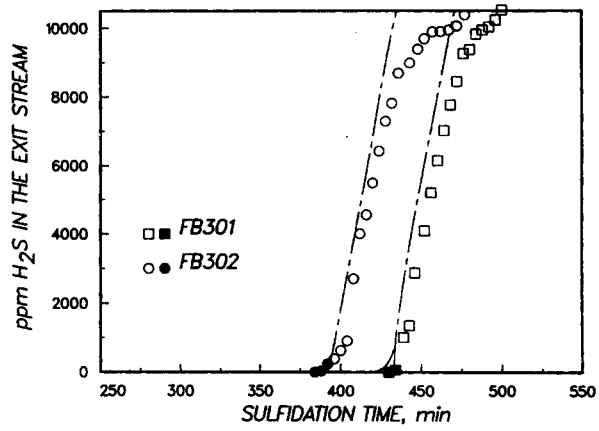

Figure 10. Comparison of the model predictions with the experimental data of two sulfidation runs at 600°C.

but since the reaction is of first-order with respect to the concentration of H_2S, results for different H_2S concentration can be compared with each other. Direct inspection of the fixed-bed model equations (Eqs. 10-16) reveals that the breakthrough curve expressed as y vs. t/t_0 is independent of the H_2S concentration at the inlet of the reactor.

It is clear from the comparison of model predictions and experimental data in Figures 7-9 that the mathematical model successfully predicts the behavior of fixed-bed reactors loaded initially with fresh (unreacted) particles. In order to examine the ability of the model to describe the behavior of a fixed-bed reactor when desulfurization starts with a nonuniform conversion profile in the bed, we carried out experiments using beds loaded with partially reacted sorbents. Specifically, we stopped the reaction in runs FB301 and FB302 after significant H_2S concentration was detected at the outlet of the reactor (a few hundred ppm, as it can be seen in Figure 9 for run FB302) by passing N_2 through the reactor. We then reversed the direction of flow in the bed and continued the sulfidation process under the reaction conditions used in the first step of the experiment. The experimental results obtained from these experiments are shown in Figure 10, with the solid markers used for the concentrations measured during the first step of the experiments. In presenting the results, the start time for the second part of the experiments was set equal to the actual time when the first sulfidation step was stopped, t^* (τ^* in dimensionless form). The model predictions of Figure 10 given by solid curves are for the first step of the experiments and were obtained by integrating the fixed-bed model equations with the initial conditions given by Eqs. 16a,b. The dashed curves give the model predictions for the second part of the experiment and were obtained by integrating the model equations with initial conditions:

$$y=0 \text{ and } \bar{\xi}=\bar{\xi}^*(x) \text{ at } \tau=\tau^* \qquad (16a,b)$$

with $\bar{\xi}^*(x)$ being the concentration profile in the inverted bed at the end of the first part of the experiment, that is, $\bar{\xi}^*(x)=\bar{\xi}(1-x,\tau^*)$. Good agreement is again observed to exist between model predictions and experimental results, especially in the most important part of the breakthrough curve, namely, that corresponding to low H_2S concentration in the outlet stream. The tendency of the mathematical model to predict sharper breakthrough curves in the high concentration region and, hence, faster completion of the reaction is due to overprediction of the reaction rate at high conversions by the particle model (see Figure 2).

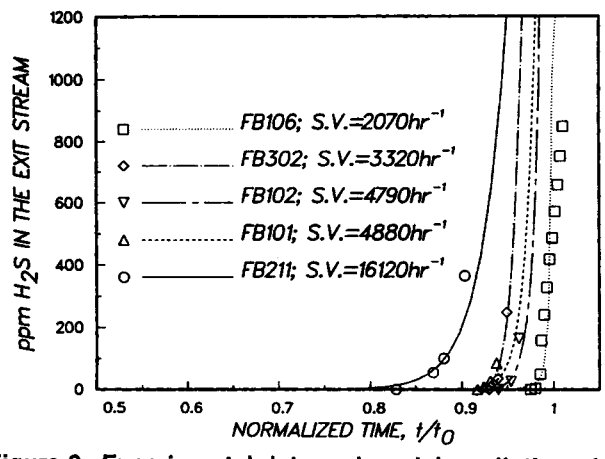

Figure 9. Experimental data and model predictions for sulfidation of the C7-2 sample at 600°C.

Analysis of the Pore Structure of the Sulfided Sorbents

The pore structure of the sulfided sorbents was characterized using mercury porosimetry and nitrogen adsorption at 77 K. Samples of reacted particles were collected from the top, bottom, and middle section of the bed. N_2 pycnometry measurements, made in the adsorption unit were used to estimate the skeletal densities of the unreacted and fully sulfided solids. Heat-treated samples of samples G-72D and C7-2 had skeletal densities of 5.4 and 4.8 g/cm^3, respectively. Lower densities were measured for the sulfided forms of the two sorbents (4 and 3.8 g/cm^3 for sorbents G-72D and C7-2, respectively).

The pore volumes of the fully sulfided sorbents agreed well with those predicted from the porosities and compositions of the unreacted (heat-treated) samples under the assumption that

there was no change in the overall dimensions of the particles during the reaction. This finding was used to determine the average conversion of the partially reacted samples using the pore volumes obtained from the mercury porosimetry data. The average conversion $\hat{\xi}$ of a sample collected between points x_1 and x_2 in the bed is obviously equal to

$$\hat{\xi} = \frac{1}{x_2 - x_1} \int_{x_1}^{x_2} \bar{\xi} dx \tag{17}$$

$\hat{\xi}$ is related to the average porosity $\hat{\epsilon}$ of the sample by the equation:

$$\hat{\xi} = \frac{\epsilon_0 - \hat{\epsilon}}{(1 - \epsilon_0)(Z - 1)} \tag{18}$$

where Z is the volume of fully reacted solid phase per unit volume of unreacted solid phase. Z is equal to 1.56 and 1.38 for samples G-72D and C7-2, respectively. The average conversion for the partially reacted samples that were collected from the top, middle, and bottom parts of the bed are shown by dashed straight lines in Figure 11 and 12 for samples G-72D (run FB209) and C7-2 (run FB211). Each dashed line extends over the portion of the bed, in terms of distance, that each average conversion represents. The continuous solid curves give the conversion profile predicted by the mathematical model at the time the sulfidation reaction was stopped. We see that in both figures the experimental average conversion histogram is in very good agreement with the theoretical conversion profile.

The cumulative pore volume vs. pore diameter curves for the partially reacted samples of Figures 11 and 12, determined from mercury intrusion porosimetry data, are given in Figures 13 and 14, respectively. Shown in the figures are also the pore-volume distribution curves for the unreacted sorbent (solid curves). The results of Figures 13 and 14 show that the total pore volume decreases with increasing conversion, while the most probable pore radius of the pore volume distributions shifts toward larger pore sizes. The decrease in the total pore volume is expected since the reaction involves a solid product (ZnS) which occupies more space than the oxide from which it results. This cannot be said, however, about the displacement of the pore-size distribution toward large pores. If the pore structure of the sorbents evolves only because of the reaction of H_2S with ZnO, the size of each pore should become progressively smaller as ZnO is replaced by ZnS and the pore-volume distribution should move toward smaller pores. Shift of the pore-size distribution toward larger pores was also observed by Grindley (1988), who performed mercury porosimetry measurements on sulfided and regenerated zinc ferrite pellets in a fixed-bed reactor.

The behavior of the pore-volume distribution curves of Figures 13 and 14 is in disagreement with the results we obtained in another study (Efthimiadis and Sotirchos, 1992b) on the evolution with the conversion of the pore-volume distribution of partially reacted samples of the same sorbents prepared in a fluidized-bed reactor. Pore-volume distribution curves for partially reacted and fully sulfided samples of sorbent C7-2 from that study are shown in Figure 15. These samples were prepared using the experimental arrangement of Figure 1 with

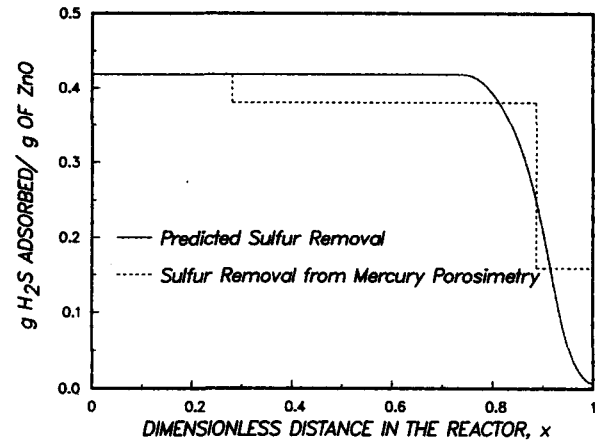

Figure 11. Comparison of the predicted by the mathematical model conversion profile in the sorbent bed of the FB209 run (sample G-72D) and the experimentally determined average conversion of segments of the sorbent bed.

the fixed-bed replaced by a fluidized-bed reactor. Specifically, about 5 g of 710–850 μm particles were sulfided up to four different conversion levels using 1.05% H_2S in N_2 flowing at 3.5 L/min (standard temperature and pressure). The pore-volume distribution of the unreacted sorbent and of the fully sulfided sorbent in the fixed-bed reactor (see Figure 14) are also shown in Figure 15 for comparison. As the results of Figure 15 show there is no shift of the pore-volume distribution of the samples prepared in the fluidized-bed reactor toward larger pores. Actually, all samples appear to have similar cumulative pore-volume distributions in the region of large pores.

All particles in a fluidized-bed reactor experience, on the average, the same reaction conditions, and as a result, partially reacted samples prepared in such a reactor consist of particles of the same conversion. Samples collected from a fixed-bed reactor, on the other hand, cover a range of conversion levels,

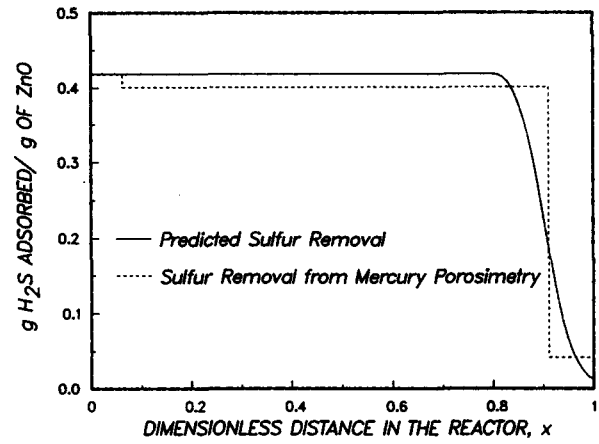

Figure 12. Comparison of the predicted by the mathematical model conversion profile in the sorbent bed of the FB211 run (sample C7-2) and the experimentally determined average conversion of segments of the sorbent bed.

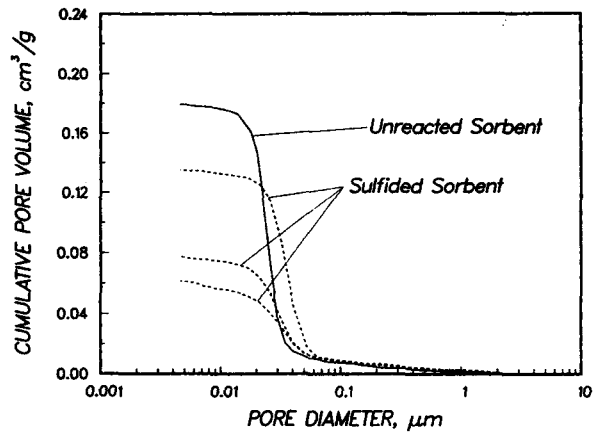

Figure 13. Porosimetric cumulative pore volume vs. pore diameter curves of unreacted G-72D sorbent and those of solid samples collected from the top, middle, and bottom of the sorbent bed of run FB209.

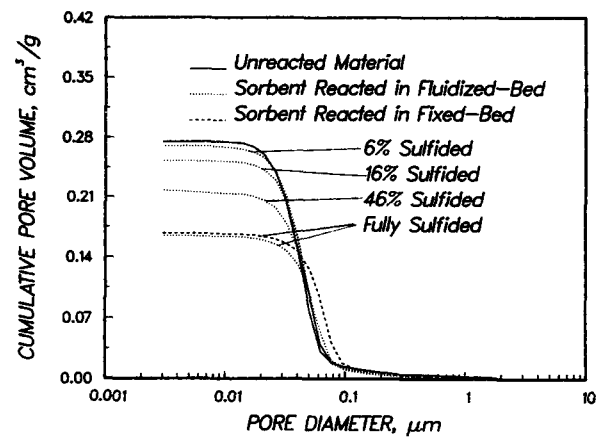

Figure 15. Pore-volume distributions of sample C7-2 sulfided in a fluidized and in fixed-bed reactor.

which may be rather broad depending on the part of the bed they were taken from (see Figures 11 and 12). This difference is important when comparing the pore-volume distributions of partially reacted samples of the same conversion from the two reactors, but it alone cannot explain the observed shift of the pore-volume distribution of the fixed-bed samples toward large pores. However, since no mixing takes place in the fixed-bed reactor, with the exception of the layer of particles located at the entrance of the reactor all other particles see the reactive mixture for the first time after they spend some time—which is roughly proportional to their distance from the entrance in the reactor—exposed to the product stream of the reaction, namely, a stream containing a % H_2O for a reactive mixture containing a % H_2S. Analysis of the pore structure of C7-2 particles (710–850 μm) exposed at 600°C to a stream containing 1% H_2O for 2 h showed shifting of the pore-size distribution towards larger pores, though to a less extent than in Figure

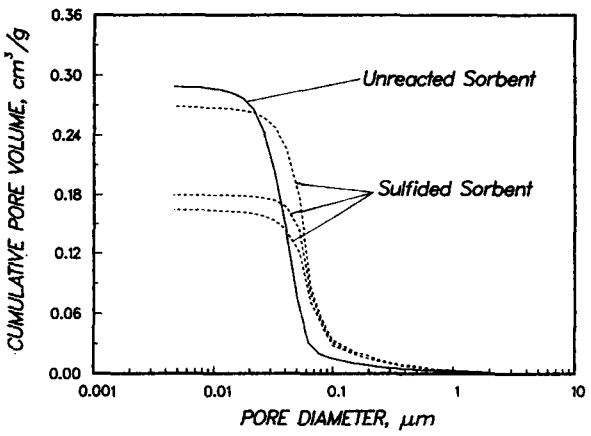

Figure 14. Porosimetric cumulative pore volume vs. pore diameter curves of unreacted C7-2 sorbent and those of solid samples collected from the top, middle, and bottom of the sorbent bed of run FB211.

13. In view of this finding, we believe that the displacement of the pore-size distributions of the fixed-bed samples toward large pores is caused by structural changes occurring because of the exposure of the sorbent particles to water vapor. Water vapor is also present in the fluidized-bed reactor, but since the internal surface of all particles is covered by a progressively thicker layer of sulfided phase, the occurring structural changes are less extensive.

The initial pore-size distributions used in the application of the mathematical model (solid curves of Figures 13 and 14) give pore surface areas 22 and 23 m^2/g, for sorbent G-72D and C7-2, respectively (pores greater than 50 Å in radius). These values are close to the BET surface areas of the unreacted materials (see Table 1). BET surface areas of fully sulfided samples of the two sorbents are listed in Table 3. The generalized pore model predicts that the surface area of the fully sulfided G-72D and C7-2 sorbents should be 16 and 18 m^2/g, respectively. The smaller experimental values of internal surface area for the sulfided sorbents are not unexpected considering the displacement of the experimental pore-volume distributions toward larger pores. Another reason for this discrepancy may be the use of the pore-size distribution extracted from mercury intrusion data in the mathematical model. This distribution corresponds to the true pore-size distribution only for an ideal structure of infinitely long cylindrical pores. For an arbitrary structure, it gives a measure of the distribution of feeder pores through which mercury invades the interior of the sorbent, and as a result it is narrower and located at smaller pore sizes than the actual pore-size distribution of the solid.

Summary and Conclusions

Two commercially available zinc oxide sorbents were reacted

Table 3. BET Surface Areas of Fully Sulfided Zinc Oxide Sorbents

Material	Experiment	Surface Area, m^2/g
G-72D	FB209	9.4
G-72D	FB212	7.9
C7-2	FB211	13.55
C7-2	FB101	15.83
C7-2	FB102	13.62

at high temperatures using H_2S-N_2 mixtures in a fixed-bed reactor. Particles in the size range of 210–850 μm were used in the experiments. Breakthrough curves were determined experimentally by chromatographic analysis of the stream leaving the reactor. The comparison of experimental data obtained under the same sulfidation conditions for the two sorbents showed that the pore structure of the sorbents plays a major role in determining sorbent utilization in the bed at the breakthrough point. Other parameters having strong effects on the behavior of the reactor were the size of the particles and the residence time of the reactive mixture in the reactor. Experiments at 500 and 600°C showed that the reaction temperature influenced insignificantly the performance of the two solids as sorbents for H_2S removal.

Samples of fully or partially reacted particles collected from different parts of the fluidized-bed reactor were analyzed by mercury porosimetry and gas adsorption. The pore-volume distribution of the reacted (partially and fully) samples was found to be shifted toward larger pores relative to the distribution of the unreacted solids. Such behavior was not seen in solids sulfided in a fluidized-bed reactor under the same conditions (temperature, pressure, and reactive gas mixture composition) as in the fixed-bed experiments. Since the particles in a fluidized-bed reactor remain exposed to the product stream of the reaction until the reaction front reaches them, it is believed that the displacement of their pore-size distribution toward larger pores is caused by structural changes occurring because of their exposure in the water vapor produced by the sulfidation reaction.

The experimental results (breakthrough curves and pore structure data) were used to test the predictions of a mathematical model for fixed-bed desulfurization reactors. The behavior of each particle in the fixed-bed reactor was described using the generalized random pore model of Yu and Sotirchos (1987). Reactivity evolution data from thermogravimetric analysis experiments had been used in a past study to determine the values of the various parameters appearing in the generalized random pore model for each of the sorbents, and as a result, the application of the overall model to the fixed-bed data involved no unknown parameters. Very good agreement was observed between model predictions and experimental data for all cases examined in our study. The mathematical model reproduced successfully both the breakthrough curves and the solid conversion profiles in the fixed-bed reactor.

It must be pointed out that it is not necessary to use a detailed model, like the one employed in this study, to describe the transport, reaction, and structure evolution processes in the pellets if our only objective is to use the overall mathematical model to correlate the experimental data. Since the general shape of the breakthrough curve is weakly influenced by the detail built into the pellet model, any model would succeed in reproducing the experimental curves provided that its parameters are allowed to vary from one experiment to another. For instance, Wang et al. (1990) used the unreacted-core model to describe the behavior of each pellet and obtained very good agreement between model results and experimental data from a bench-scale reactor loaded with zinc ferrite or zinc titanate pellets. However, the effective diffusivity values that had to be used to obtain good agreement between model and experiment were much different from those used in another study (Woods et al., 1991) to reproduce, using the unreacted-core model, sulfidation data for single pellets of the same sorbents from gravimetric experiments.

Acknowledgment

This work has been supported by a grant from the U.S. Dept. of Energy. The pore structure of the ZnO sorbents was characterized using equipment acquired through an NSF equipment grant.

Notation

Symbols that do not appear here are defined in the text.

a = radius of the particle, cm
c = reactive gas concentration in the bed, mol/cm^3
c_0 = initial reactive gas concentration in the bed, mol/cm^3
c_b = reactive gas concentration in the bulk phase, mol/cm^3
c_p = reactive gas concentration in the particle, mol/cm^3
$\mathfrak{D}$ = bulk diffusion coefficient, cm^2/s
D_b = axial dispersion coefficient in the fixed bed, cm^2/s
D^e = effective diffusion coefficient in the particle, cm^2/s
D_0^e = initial effective diffusion coefficient in the particle, cm^2/s
k_g = mass-transfer coefficient, cm/s
k_s = reaction rate constant in the particle, cm/s
k_v = volumetric reaction rate constant in the particle, s^{-1}
k_{v0} = initial volumetric reaction rate constant in the particle, s^{-1}
$\bar{k}_v$ = average volumetric reaction rate constant in a particle or in the bed, s^{-1}
L = length of the sorbent bed, cm
Pe = Peclet number (see Eq. 12c)
r = radial distance in a particle, cm
$\bar{R}_v$ = average reaction rate per unit of particle volume, mol/cm^3/s
S_0 = initial surface area, cm^2/cm^3
Sh^e = Sherwood number (see Eq. 6c)
t = time, s
t_0 = minimum time for the complete conversion of the sorbent bed, s
u = superficial velocity in the reactor, cm/s
v_s = volume of the unreacted solid per mol of the solid reactant, cm^3/mol
x = dimensionless distance in the bed
x_i = dimensionless distance of point i in the bed
y = dimensionless concentration in the bed
y_p = dimensionless concentration in the particle
z = axial distance in the bed, cm
Z = volume of fully reacted solid phase per unit volume of unreacted solid phase

Greek letters

δ^e = dimensionless effective diffusivity
ϵ_0 = porosity of the unreacted particles
ϵ_b = bed voidage
ϵ_p = porosity of the reacted particles
$\bar{\epsilon}$ = average porosity of particles located in a segment of the sorbent bed
η = tortuosity factor for axial dispersion
κ_v = dimensionless reaction rate constant in a particle
ν_A = stoichiometric coefficient of the reactive gas
ξ = local solid conversion in a particle
$\bar{\xi}$ = average solid conversion in a particle or in the bed
$\hat{\xi}$ = average conversion of particles located in a segment of the fixed-bed
ρ = dimensionless distance in a particle
τ = dimensionless time for the fixed-bed reactor (see Eq. 13a)
τ_p = dimensionless time for the particle (see Eq. 6a)
Φ^2 = Thiele modulus for the particle (see Eq. 6b)
$\bar{\Phi}^2$ = Thiele modulus for the sorbent bed (see Eq. 13b)
ω = dimensionless parameter (see Eq. 13c)
ω_p = dimensionless parameter (see Eq. 5e)

Literature Cited

Barin, I., and O. Knacke, *Thermochemical Properties of Inorganic Substances*, Springer-Verlag, New York (1973).

De Boer, J. H., B. G. Linsen, T. Van Der Plas, and G. J. Zondervan, "Studies on Pore Systems in Catalysts. VII. Description of the Pore Dimensions of Carbon Blacks by the t-method," *J. Catalysis*, **4**, 649 (1965).

Caillet, D. A., and D. P. Harrison, "Structural Property Variations in the MnO-MnS System," *Chem. Eng. Sci.*, **37**, 625 (1982).

Dixon, A. G., "Correlations for Wall and Particle Shape Effects on Fixed Bed Bulk Voidage," *Can. J. Chem. Eng.*, **66**, 705 (1988).

Efthimiadis, E. A., and S. V. Sotirchos, "Reactivity Evolution during Sulfidation of Porous Zinc Oxide," *Chem. Eng. Sci.*, submitted (1992a).

Efthimiadis, E. A., and S. V. Sotirchos, "Effects of Pore Structure on the Performance of Coal Gas Desulfurization Sorbents," *Chem. Eng. Sci.*, submitted (1992b).

Gangwal, S. K., S. M. Harkins, M. C. Woods, S. C. Jain, and S. J. Bossart, "Bench-Scale Testing of High-Temperature Desulfurization Sorbents," *Environ. Prog.*, **8**, 265 (1989).

Grindley, T., "Sidestream Zinc Ferrite Regeneration Tests," *Proceedings Annual Gasification and Gas Stream Cleanup Systems Contractors Review Meeting*, **1**, p. 58, DOE/METC/6092 (1988).

Jain, S. C., S. K. Gangwal, E. Gal, and R. E. Ayala, "A Study of the Chemical Reactivity and Mechanical Durability of High-Temperature Desulfurization Sorbents for Moving-Bed and Fluidized-Bed Applications," AIChE Meeting, San Diego (1990).

Krishnan, S. V., and S. V. Sotirchos, "Effective Diffusivity Changes During Carbonation, Recalcination, and Sulfation of Limestone Calcines," AIChE Meeting, Chicago (1990).

Lee, G. T., R. R. Gansley, and M. J. Baird, "Fluid Bed Desulfurization of Coal-Derived Gas," AIChE Meeting, San Diego (1990).

Park, H. C., S. Kimura, Y. Sakai, S. Tone, and T. Otake, "An Unsteady State Analysis of Packed Bed Reactors for Gas-Solid Reactions," *J. Chem. Eng. Japan.*, **17**, 269 (1984).

Sotirchos, S. V., and H. C. Yu, "Mathematical Modelling of Gas-Solid Reactions with Solid Product," *Chem. Eng. Sci.*, **40**, 2039 (1985).

Sotirchos, S. V., and H. C. Yu, "Overlapping Grain Models for Gas-Solid Reactions with Solid Product," *Ind. Eng. Chem. Res.*, **27**, 836 (1988).

Sotirchos, S. V., and S. Zarkanitis, "Pellet-Model Effects on Simulation Models for Fixed-Bed Desulfurization Reactors," *AIChE J.*, **35**, 1137 (1989).

Tamhankar, S. S., M. Bagajewicz, G. R. Gavalas, P. K. Sharma, and M. Flytzani-Stephanopoulos, "Mixed-Oxide Sorbents for High-Temperature Removal of Hydrogen Sulfide," *Ind. Eng. Chem. Process Des. Dev.*, **25**, 429 (1986).

Wang, J. C. P., F. R. Groves, and D. P. Harrison, "Modeling High Temperature Desulfurization in a Fixed-Bed Reactor," *Chem. Eng. Sci.*, **45**, 1693 (1990).

Woods, M. C., S. K. Gangwal, D. P. Harrison, and K. Jothimurugesan, "Kinetics of the Reactions of a Zinc Ferrite Sorbent in High-Temperature Coal Gas Desulfurization," *Ind. Eng. Chem. Res.*, **30**, 100 (1991).

Yu, H. C., and S. V. Sotirchos, "A Generalized Pore Model for Gas-Solid Reactions Exhibiting Pore Closure," *AIChE J.*, **33**, 382 (1987).

Yumura, M., and E. Furimsky, "Comparison of CaO, ZnO, and Fe_2O_3 as H_2S Adsorbents at High Temperatures," *Ind. Eng. Chem. Process Des. Dev.*, **24**, 1165 (1985).

Zarkanitis, S. E., E. A. Efthimiadis, and S. V. Sotirchos, "Experimental Evaluation of a Class of Distributed Pore Size Models for Gas-Solid Reactions with Solid Product," *Chem. Eng. Sci.*, **45**, 2761 (1990).

Manuscript received Dec. 18, 1991, and revision received June 26, 1992.